ELSEVIER

Journal of Molecular Graphics and Modelling 20 (2001) 145–154

Journal of Molecular Graphics and Modelling

www.elsevier.com/locate/JMGM

Molecular dynamics simulations of wild-type and point mutation human prion protein at normal and elevated temperature

Eman El-Bastawissy, Michael H. Knaggs, Ian H. Gilbert*

Welsh School of Pharmacy, Cardiff University, Redwood Building, King Edward VII Avenue, Cardiff CF10 3XF, UK

Received 22 March 2001; received in revised form 30 May 2001; accepted 6 June 2001

Abstract

This paper describes molecular dynamics simulations of prion protein at 300 and 500 K. This was undertaken to gain insight into the factors involved in the stability of prion protein. Simulations were done using the Particle Mesh Ewald (PME) method using a homology model of the C-terminal fragment of human prion protein and the NMR structure of the human prion protein. The simulations at both 300 and 500 K were stable. Simulations were also undertaken with a mutant known to be associated with prion disease: Asp178Asn. The Asp178Asn simulation trajectory was observed to be much less stable than for the wild-type protein trajectory. Significant breakdown in secondary structure was observed for Asp178Asn at 500 K.

Keywords: Prion protein; Simulation; NMR structure

1. Introduction

Transmissible spongiform encephalopathies (TSEs) are an unusual class of neurodegenerative diseases, which are fatal and for which there is no known treatment. Examples of the disease are scrapie in sheep, bovine spongiform encephalopathy (BSE) in cattle and in humans, Creutzfeld Jacob disease (CJD), Gerstmann Straussler Scheinker syndrome (GSS), kuru and fatal familial insomnia (FFI). In humans, CJD can be sporadic, familial, iatrogenic or due to infection. Associated with TSEs is an accumulation of amyloid deposits, vacuolation and astroglial proliferation in the brain. There has been an increase in interest in these diseases due to a new form of CJD in humans, the so-called variant CJD [1,2].

The infectious agent in TSEs is believed to be or is associated with abnormally folded prion protein (PrP-res). Normal prion protein, PrP^C, is a GPI-anchored sialoglycoprotein (194–218 residues in the mature protein depending on species) [3,4] naturally occurring throughout the body, but especially in the central nervous system. The precise role of the normal protein is unknown. The NMR structures of fragments of the mouse, [5,6] hamster [7], human [8] and bovine [9] prions have been determined. Recently, the NMR structure of some single-residue variants of the human prion protein have been determined as well [10].

In the NMR structures of the prion protein, the N-terminal end is generally disordered. It has been speculated that in solution, this may be complexed to copper ions [11]. In contrast, the C-terminal end is well ordered and structured. The structure of this C-terminal section is very similar for all four proteins. Essentially, it consists of three α-helices (144–153 (helix 1), 172–194 (helix 2) and 200–228 (helix 3 (human numbering))) and a short two-strand β-sheet (129–131 and 161–163) (Fig. 1 of human NMR structure and Table 1). (The definitions of α-helices and β-sheets used here are those defined in the MOLMOL software package [12]. In the paper of the mouse NMR structure [5], different definitions are used to describe the secondary structure.) The main difference between the mouse prion and the human NMR structures is that helix 3 in the human prion is longer than that of the mouse prion and there is a bend in the mouse prion in helix 3 starting from residue 217.

There is no known chemical difference between the normal cellular form of the prion protein (PrP^C) and the abnormal form of the prion protein (PrP-res) [4,13], and the difference appears to be a conformational change. PrP^C is predominantly alpha helical in structure, whilst the abnormal form has a high β-sheet content [14]. In addition, the abnormal form has an unusual resistance to degradation by proteinase K at the C-terminal end [14,15]. The precise mechanism by which the normal prion protein is converted to the abnormal prion protein is not known. However, it is

* Corresponding author. Tel.: +44-29-2087-5800; fax: +44-29-2087-4149.
E-mail address: gilbertih@cf.ac.uk (I.H. Gilbert).

1093-3263/01/$ – see front matter
PII: S1093-3263(01)00113-9

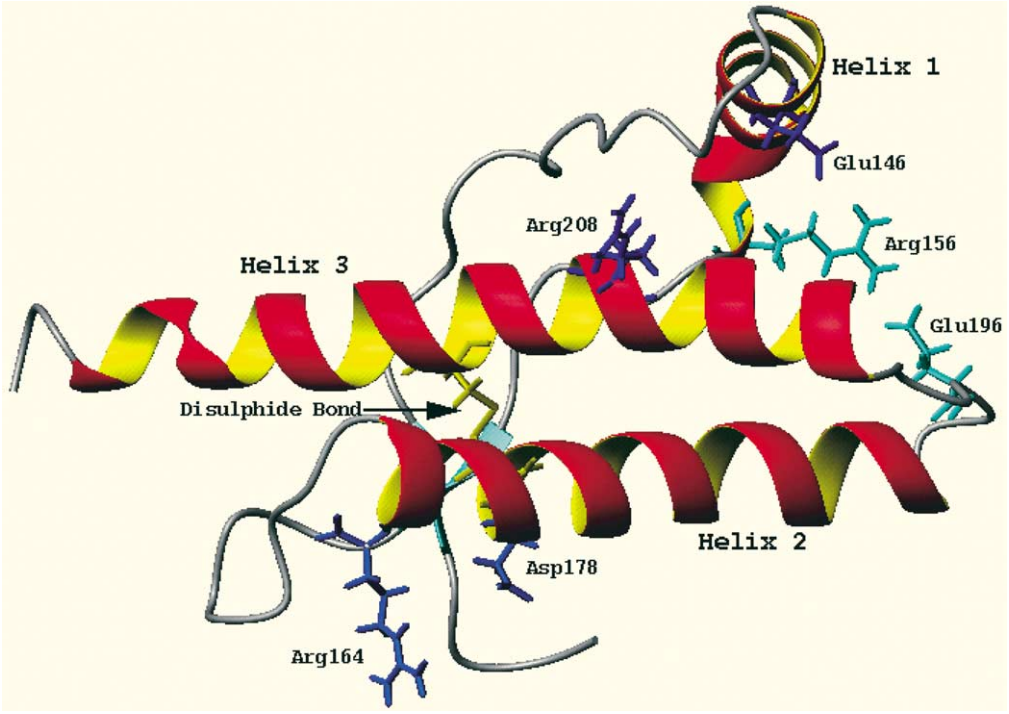

Fig. 1. The Ribbon diagram of the human prion NMR structure (figure created with MOLMOL).

believed that there may be interaction between PrP^C and PrP-res leading to conversion of PrP^C to PrP-res [14–17]. This process may or may not require the presence of a chaperone protein [18–20].

We were interested in investigating the factors involved in the stabilisation and destabilisation of prion proteins. We have done this using molecular dynamics (MD) simulations which allow calculation and investigation of the conformational characteristics of the protein at every step during the simulation [21]. It was anticipated that the use of high temperatures should cause some unfolding of the protein during the simulation and may give information about the unfolding pathway [22]. In addition, the effect of Asp178Asn mutation on the human prion protein stability was investigated. As Asp178 (in the middle of helix 2) makes a salt bridge with Arg164 in strand 2, so mutation of this residue could effect the salt bridge and may have a crucial role in protein stability [23].

Several studies have been reported on molecular dynamics simulations on prion protein [23–26]. These studies have been undertaken using the mouse or hamster NMR structures and a homology model of the human structure at room temperature. Work by Zuegg and Greedy [23] found that the PME method gave the simulation with the greatest stability.

Table 1
Secondary structure elements of the prion protein as defined by MOLMOL following PME simulations

	Strand1	Strand2	Helix 1	Helix 2	Helix 3	3_{10}-helix
Mouse prion NMR structure[a]	128–131	161–164	144–154	179–193	200–217	
Mouse prion NMR structure (1ag2)[b]	129–131	161–163	144–153	172–192	200–222	
Human homology model	129–131	161–163	144–153	172–192	200–222	
Homology model Average[c] structure at 300 K	129–131	161–163	144–153	173–193	200–216, 219–222	154–156
Homology model average structure at 500 K	129–131	161–163	144–153	172–193	200–225	154–156
Human prion NMR structure	129–131	161–163	144–153	172–193	200–228	154–156
Human prion NMR average structure at 300 K	129–131	161–163	144–153	172–193	200–227	154–156
Human prion NMR average structure at 500 K	129–131	161–163	144–153	172–193	200–228	154–156
Asp178Asn mutant model (from human NMR structure)	129–131	161–163	144–153	172–193	200–228	154–156
Asp178Asn mutant average structure at 300 K	128–133	160–164	144–153	172–193	200–227	154–156
Asp178Asn mutant average structure at 500 K	128–133	160–164	144–153	172–193	200–227	

[a] The secondary structures defined by Riek et al. [5].
[b] The secondary structures defined by MOLMOL using the pdb file 1ag2.
[c] The average structure means the whole simulation average structure.

When this work was commenced, the structure of the human prion was not available and initial work was done with a homology model using the mouse NMR structure as a template. Work with mutants was then carried out using the human NMR structure. The dynamics simulations concentrated on the C-terminal end of the protein, which is believed to be important in the transition from the normal to abnormal form of the protein and most mutations associated with increased incidence of prion diseases are found within this part of the protein. The flexible N-terminal region appears to have a negligible effect on the structure of the C-terminal core [6,8].

2. Methodology

2.1. Homology modelling

The homology model of the human prion protein was constructed using the COMPOSER module within SYBYL 6.5 suite of programmes [27].

The systems investigated in the simulations were minimised and equilibriated prior to the production molecular dynamics simulation in order to remove any bad contacts, and to optimise solvent–protein interactions. The protonation states for the charged residues in the protein structure were set to those expected at pH 7. The protein structure (either homology model, or NMR structure) was subjected to 1000 steps of conjugate gradient minimisation using the AMBER 5.0 suite of programmes [28,29] and AMBER 94 force field [30].

For the Particle Mesh Ewald (PME) and counter-ion cut-off simulations, uncharged systems were required. This was achieved by the addition of sodium ions to balance the charge of the protein. The minimised structure, with counter-ions, was then solvated in a rectangular box of pre-equilibriated TIP3P water molecules [31] which extended 8 Å × 8 Å × 8 Å further than the protein atoms. The resulting system was then minimised using conjugate gradient minimisation for a further 1500 cycles.

2.2. Equilibriation

The systems under investigation (Table 2) were equilibriated for 25 ps using the constant pressure and temperature (NPT) algorithm of Berendsen et al. [32] with coupling constants of 0.2 ps for both solute and solvent atoms. The SHAKE algorithm [33] was used during the equilibriation stage with a time step of 2 fs. The equilibrations were performed at 300 K with a non-bonded cut-off of 10 Å and a dielectric constant of 1.

2.3. MD simulations

The outputs of the equilibrated phase were used as input for the main simulations. The SHAKE algorithm was used on bonds involving hydrogen atom and a time step of 2 fs was used. Constant volume and temperature (NTV) and periodic boundary conditions were used in all simulations. Non-bonded interactions upto 10 Å were taken account of in the cut-off method. For the PME method, a grid of suitable size (slightly bigger than the water box size) was used to calculate the long-range electrostatic interactions. The structures were saved every 1 ps. The details of each simulation are summarised in Table 1.

All the simulations were performed on Silicon Graphics O2 and Indigo 2 workstations running irix 6.5.

3. Results

Initial work was carried out using a homology model of the prion protein prepared from the mouse NMR structure [5]. This structure was used to establish that the Particle Mesh Ewald method was the most stable method for simulation. During the course of the work, an NMR structure of the human prion protein was published [8] and this was used for further work. The homology model was very similar to the mouse template with a backbone RMSD (root mean square deviation) of 0.06 Å. We have subsequently compared the secondary structure elements of our homology model with the published structure of the human prion protein. The only apparent difference occurs in helix 3, which is longer in the NMR structure of the human prion protein (Table 1). The backbone RMSD of the homology model was 3.32 Å from the human NMR structure.

3.1. Simulations of human prion protein homology model

3.1.1. Cut-off and counter ion methods

Simulations were undertaken with the cut-off and counter ion methods using the homology model of the human prion

Table 2
Simulations performed

Protein	No. of Na^+ ions	Box dimensions ($Å^3$)	Ewald grid box dimension ($Å^3$)	No. of water molecules	Non-bonded cut-off (Å)	Electrostatic method
Wild-type homology model	0	53.23 × 46.81 × 39.81		3363	10	Cut-off
Wild-type homology model	4	53.31 × 52.39 × 40.82		3350	10	Cut-off
Wild-type homology model	4	53.31 × 52.39 × 40.82	56 × 54 × 42	3350	10	PME
Wild-type NMR structure	3	62.27 × 49.05 × 43.70	64 × 52 × 46	3980	10	PME
Asp178Asn mutant model	2	63.86 × 47.65 × 44.65	66 × 50 × 46	4021	10	PME

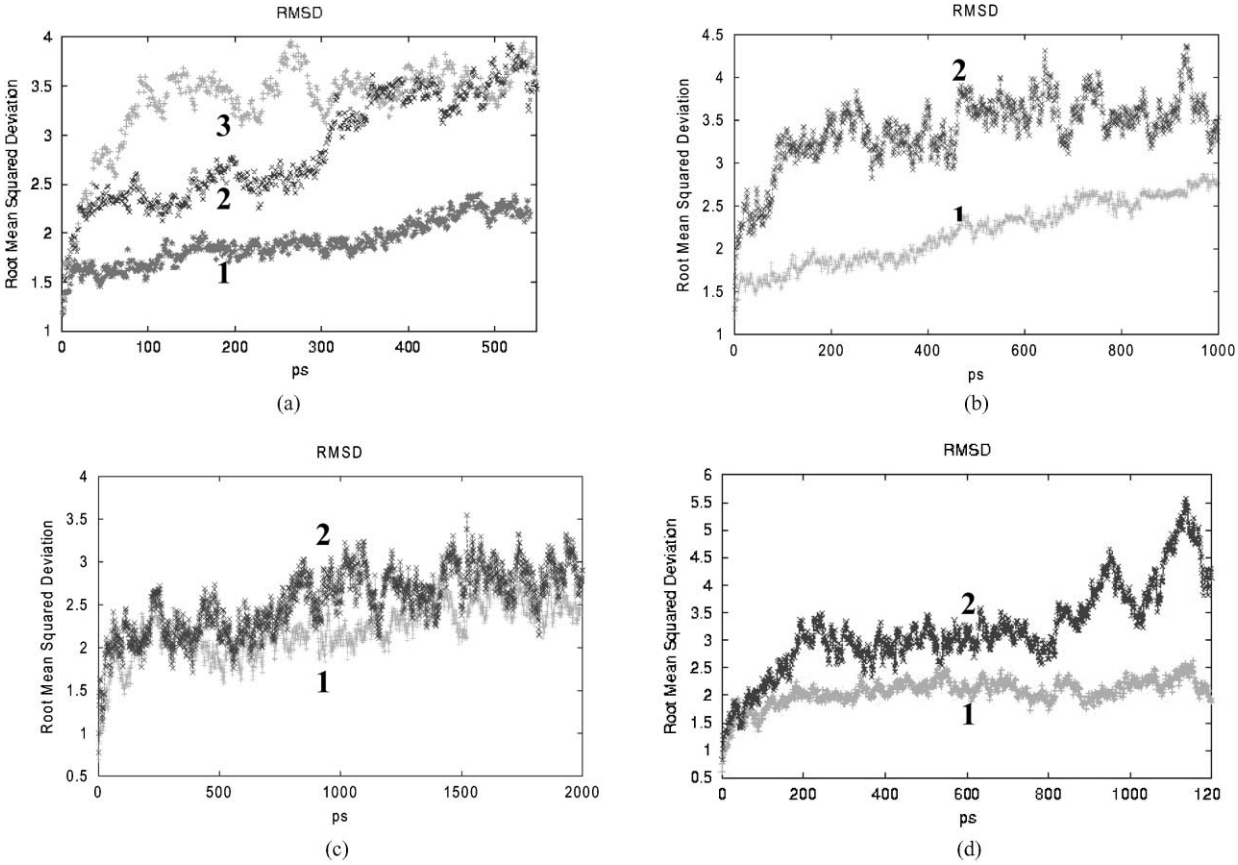

Fig. 2. The RMSD as a function of simulation time. (a) Normal prion at 300 K: (1) PME simulation; (2) counter ion simulation; (3) cut-off simulation. (b) Normal prion homology model: (1) at 300 K; (2) at 500 K using PME method. (c) Human prion NMR structure: (1) at 300 K; (2) at 500 K using PME method. (d) Asp178Asn mutant: (1) at 300 K; (2) at 500 K using PME method.

protein at 300 K. However, neither of these methods appeared to produce reliable models. In the case of the cut-off method, the Cα RMSD was high (3.9 Å) and showed large variation (Fig. 2a, trace 3); helix 1 was absent for most of the simulation (Fig. 3a) and for some of the time helix 3 underwent breakdown and conversion to a 3_{10}-helix. The cut-off simulations were then repeated (counter ion method) using four sodium ions to neutralise the system as it has been reported that salt ions increase the stability of the protein in MD simulations [34]. Again the Cα RMSD (Fig. 2a, trace 2) indicated instability and there was breakdown in helix 1 and changes in helix 3 (Fig. 3b). These results parallel the reports of Zuegg and Greedy [23] who found similar instability.

3.1.2. Particle Mesh Ewald method

Therefore, the PME method was used [23]. Analysis of the simulation trajectory at 300 K highlighted much higher stability of the prion model upto 1 ns (Fig. 2a, trace 1 and Fig. 2b, trace 1). The Cα RMSD was less than 2.0 Å for about

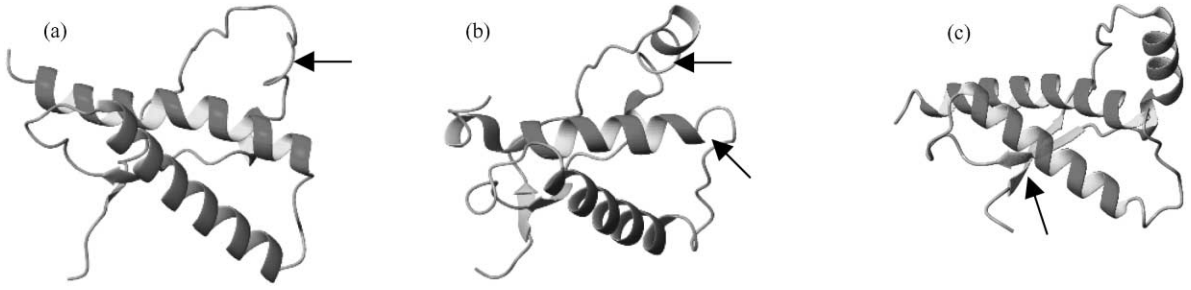

Fig. 3. Ribbon diagram of (a) the average structure of the cut-off simulation at 300 K; (b) the average structure of the counter ion simulation at 300 K; (c) the average structure from 100 to 300 ps of the human NMR structure at 500 K. The arrows indicate areas of change.

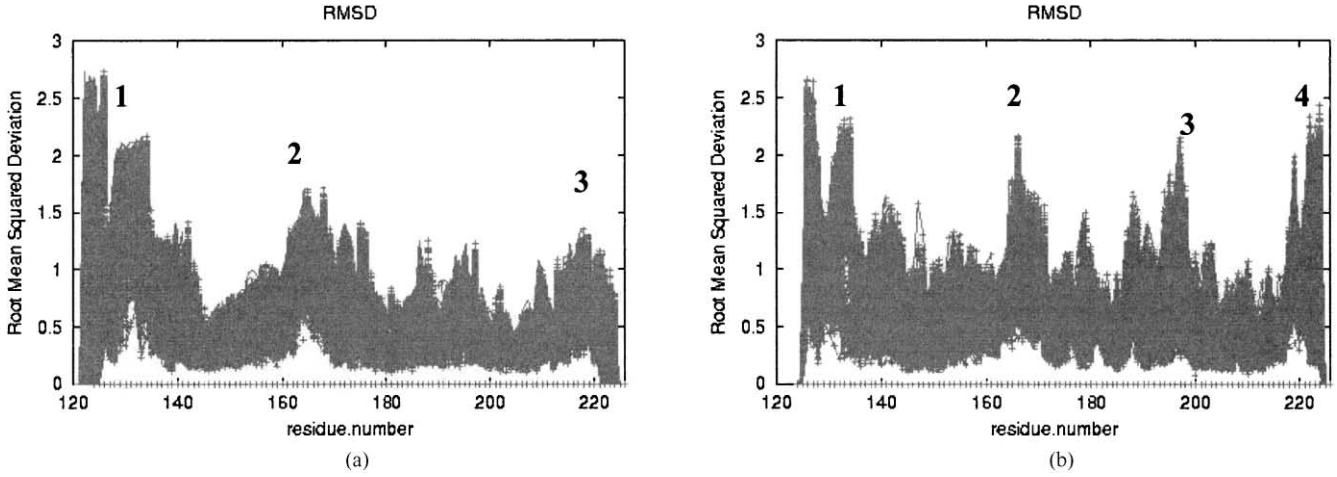

Fig. 4. Residue-based RMSD throughout the course of human homology model PME simulation. This figure monitors the movement of individual residues. Most movement occurred at (a) 300 K: (1) the N-terminal region (124–135), (2) the loop before helix 2 (164–172), (3) the C-terminal region; and (b) at 500 K: (1) the N-terminal region, (2) the loop before helix 2 (165–172), (3) the loop before helix 3 (193–199), (4) the C-terminal region of helix 3 due to elongation of the helix.

400 ps, then the RMSD rose to about 2.7 Å at the end of the simulation. Analysis of the structures and plots of α-helical and β-sheet content showed the structure to be stable with slight changes being: a small 3_{10}-helix at the end of helix 1 (154–156); a split in helix 3 (between residues 216–219) (Table 1); movement of the N-terminal region (124–135) (Fig. 4a); and movement of the loop just before helix 2 (164–172).

3.1.2.1. High temperature simulation of human homology model. We decided to investigate the effect of the high temperature on the prion protein behaviour. A temperature of 500 K was used; at this temperature initial unfolding/breakdown should occur during a 1 ns simulation, whilst higher temperatures may lead to a breakdown in accuracy. The Cα RMSD increased to rapidly to 3.4–3.8 Å and remained at this level for most of the simulation (Fig. 2b, trace 2). The α-helical and β-sheet showed little structural change. However, helix 3 became longer and straighter during the simulation. The elongation led to the gain of more interactions between the C-terminal region of helix 3 and the region around the beginning of helix 2. There was a clear hydrophobic interaction between the phenyl ring of Tyr218 and the carbon skeleton of Gln172 (the closest carbon atoms are 2.99 and 3.2 Å from the phenyl carbons) and a hydrogen bond between the phenolic hydrogen of Tyr218 and the hydroxyl oxygen of Ser170 (distance of 1.78 Å). These interactions are absent in both the mouse NMR structure and the human homology model, but present in the human NMR structure. Other small changes are as follows: a small 3_{10}-helix at 154–156 at the C-terminal end of helix 1 as is found in the NMR structure of the human prion (Table 1); movements of the N-terminal region (124–135); the loop before helix 2 (165–172); and the loop before helix 3 (193–199) as well as the C-terminal region of helix 3 (Fig. 4b). Therefore, the dynamics simulations predict movement of the loops. Experimentally, the flexibility of some loops can be seen by studying the NMR structures of the human prion protein [8]. Three structures have been reported of slightly different fragments of the human prion protein: for these the secondary structural elements were superimposable, but the loops showed a degree of disorder.

The backbone RMSD of the simulation structure (averaged over 501–1000 ps) from the NMR structure of the human prion protein was 1.76 Å. This value is much lower than that of the homology model compared to the human NMR structure (3.32 Å). These data reveal that after 1000 ps simulation at 500 K, the structure of the homology model became much closer to that of the NMR structure.

3.2. PME simulations of human prion protein using the NMR structure

At 300 K, the maximum Cα RMSD was 2.5 Å using the PME simulation method, indicating the stability of the simulation (Fig. 2c, trace 1). No major changes in the helical content or the number of main chain hydrogen bonds took place during the simulation, whilst the β-sheet content showed some variation between 4 and 9% during the first half of the simulation (Fig. 5a). For the remainder of the simulation, it was at 4%. The increase in β-sheet content occurred by extension of the existing β-sheets (residues 128–133 for strand 1 and 160–164 for strand 2). Comparison of structures, averaged over 100 ps, showed little variation in secondary structure. The radius of gyration oscillated between 14.8 and 15.2 Å, indicating that very little change took place in the protein tertiary structure and it remained compact during the simulation. Because of its stability, the 300 K NMR simulation could be used as a reference for the high temperature unfolding simulation.

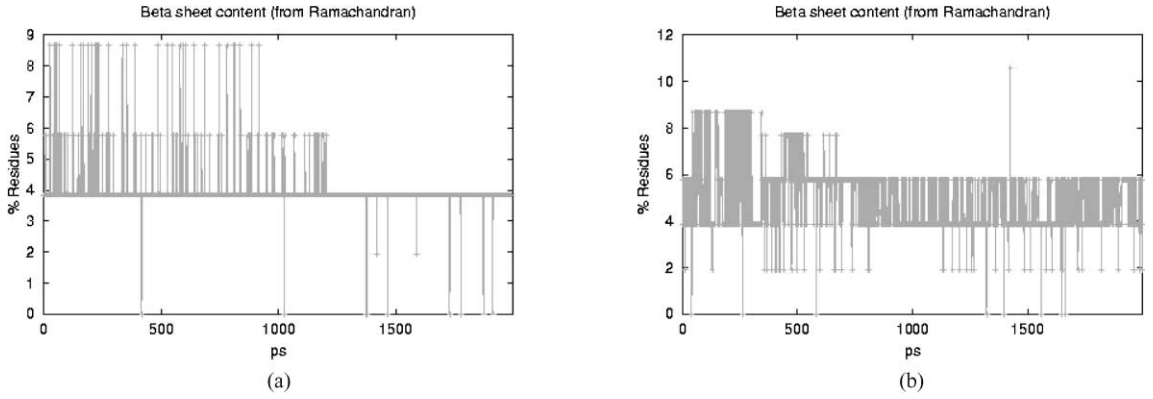

Fig. 5. Analysis of the β-sheet content as a function of simulation time of the prion protein wild type NMR structure: (a) simulation at 300 K; (b) simulation at 500 K.

The simulation at 500 K (Fig. 2c, trace 2) showed little variation compared to the simulation at 300 K. Some of the possible reasons for this are discussed later. Essentially the Cα RMSD oscillated between 2.0 and 2.5 Å in the first half of the simulation. Thereafter, it rose up and fluctuated between 2.5 and 3.0 Å to the end of the simulation. The helical content remained constant during the simulation. However, the β-sheet content was again higher (8.5%) in the initial period (50–300 ps) of the simulation compared to 4–6% during the rest of the simulation as shown in Fig. 5b. This was due to elongation of the β-sheets and was more pronounced at 500 K than at 300 K. However, this effect disappeared in the second half of the simulation. Guilbert et al. [24] found an extra strand in the same area of the β-sheet on their mouse prion simulation. Comparing time-averaged structures (over 100 ps intervals), no major changes in secondary structure were observed except the elongation of the β-sheet in the period from 100 to 300 ps (Fig. 3c).

3.3. PME simulations of human prion protein Asp178Asn mutant

The Asp178Asn mutant simulation was carried out at 300 K using the PME method. The Cα RMSD increased to about 2 Å during the first 200 ps of the simulation and then remained stable for the rest of the simulation, varying between 2.0 and 2.3 Å (Fig. 2d, trace 1). The alpha helical content remained reasonably constant at 54–59%. The β-sheet content showed a lot more variation (Fig. 6a), oscillating between 4 and 9% throughout the simulation. Studying time-averaged structures (over 100 ps intervals) confirmed the stability of the helical structure and elongation of the β-sheets to include residues 128–133 for strand 1 and 160–164 for strand 2. Visualisation of the RMSD of individual residues throughout the simulation is shown in Fig. 7a. Essentially, most of the changes occurred in the N-terminal region (124–135). The other area showing significant variation is the loop (164–172) just before helix 2. The region of the α-helices showed much less mobility.

At 500 K, the Cα RMSD rose to about 3 Å over the first 200 ps of the simulation and oscillated between 2.8 and 3.2 Å for 600 ps. Thereafter, it recorded a sharp rise to about 4.5 Å at 950 ps and another rise to 5.5 Å after 1150 ps (Fig. 2d trace 2). The rise in RMSD indicates large changes to the protein structure. The radius of gyration increased, particularly during the last 400 ps of the simulation (Fig. 6c), suggesting some disruption of the tertiary structure of the protein. The alpha helical content remained constant during the simulation. However, the β-sheet content increased during the simulation (Fig. 6b). By studying time-averaged structures of the protein (averaged over 100 ps), the increased in β-sheet content could be attributed to elongation of the existing sheets. There were also large changes in the loop just before helix 1 which moved away from helix 1 leaving a big gap in the protein tertiary structure (Fig. 8). The conformation of the loop connecting helix 2 with helix 3 was also changed and as a result helix 3 moved closer to helix 2 and further away from helix 1 leading to another gap in the tertiary structure of the prion protein. Studying the RMSD of individual residues throughout the simulation (Fig. 7b) indicated significantly more motion of certain regions. The loops between strand 1 and helix 1; strand 2 and helix 2; and helix 2 and helix 3 showed most variation together with the C-terminal region of helix 3.

During the simulation of the NMR structure of the wild-type human prion, a salt bridge formed between Arg164 and Asp178. In the Asp178Asn mutant, this salt bridge can no longer form. In the starting structure of the mutant, there is a hydrogen bond between the side chain carbonyl of Asn178 and the guanidine side group of Arg164. During the simulation at both 300 and 500 K, this hydrogen bond disappeared. However, there still appeared to be a hydrophobic interaction between the side chains of Asn178 and Arg164 after the hydrogen bond had disappeared. Similarly, another hydrogen bond present in the human NMR structure and the starting structure for simulation of the mutant (between the OH group of Tyr128 and the side chain amide of Asn178) disappeared during the simulation. One

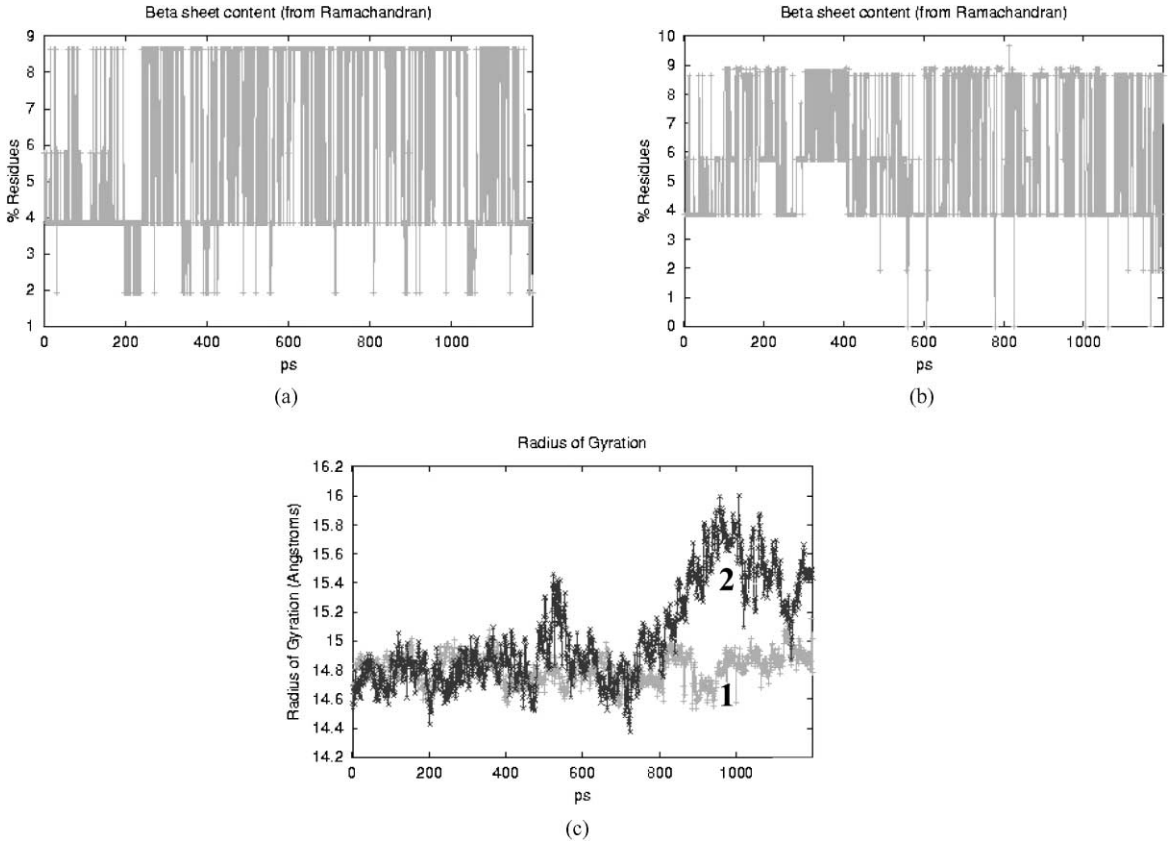

Fig. 6. Analysis of the simulation trajectory as a function of simulation time of the Asp178Asn mutant model: (a) a plot of the β-sheet content as a function of simulation time at 300 K; (b) a plot of the β-sheet content as a function of simulation time at 500 K; (c) radius of gyration as a function of simulation time. Trace 1 is for the 300 K simulation; trace 2 is for the 500 K simulation.

of the cysteine residues forming the disulfide bond is close to the site of the mutation. This bond was nearly conserved throughout the simulations at both 300 and 500 K.

3.3.1. Summary of the Asp178Asn mutant simulation

At 300 K, the simulation trajectory was reasonably stable (low RMSD, constant number of main chain hydrogen bonds, low radius of gyration changes, and the stable helical structure). However, even at early stages of the simulation, the β-sheet elongated (strand 1 from 128 to 133 instead of from 129 to 131 and strand 2 from 160 to 164 instead of from 161 to 163). This was due to a conformational change allowing more interaction between strand 1 (128–132) and strand 2 (160–164), leading to an extension of the β-sheet.

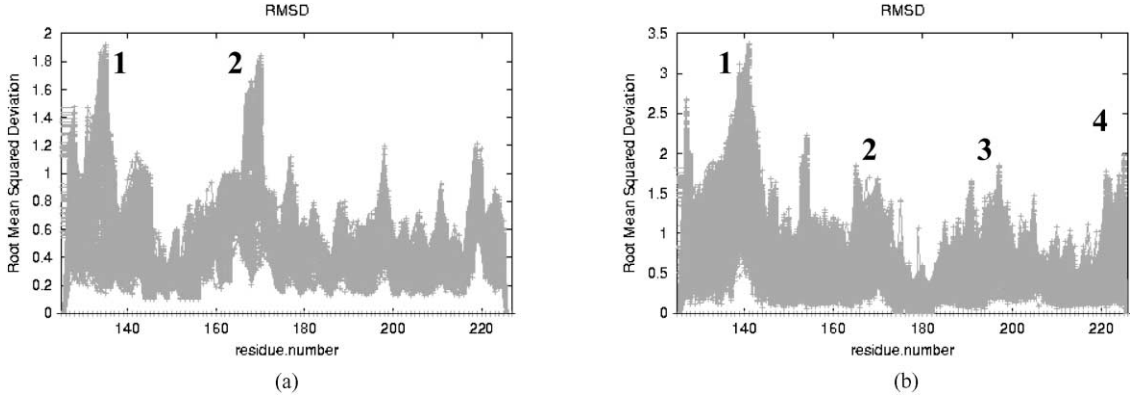

Fig. 7. Residue-based RMSD throughout the course of Asp178Asn mutant simulation. Most of the variation occurred (a) at 300 K: (1) the N-terminal region (124–135), (2) the loop before helix 2 (164–172); and (b) at 500 K: (1) the loop between strand 1 and helix 1 (139–144), (2) the loop before helix 2 (164–172), (3) the loop before helix 3, (4) the C-terminal region of helix 3.

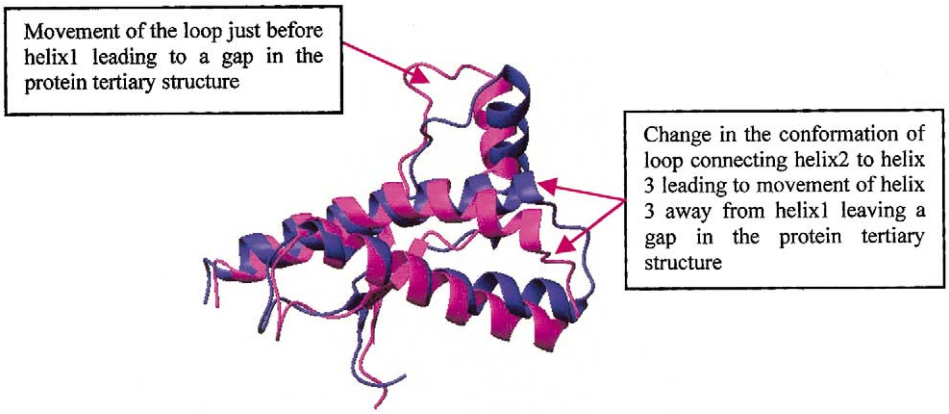

Fig. 8. Ribbon diagram of the superimposed secondary structure of the Asp178Asn mutant average structure for the last 200 ps of the 500 K simulation (magenta colour), and that of the starting structure (blue colour) showing the movement of the loop just before helix 1 away from it leading to a gap in the protein tertiary structure and the conformational change that took place to the loop connecting helix 2 to helix 3 which led to movement of helix 3 away from helix 1 leaving another gap in the protein tertiary structure.

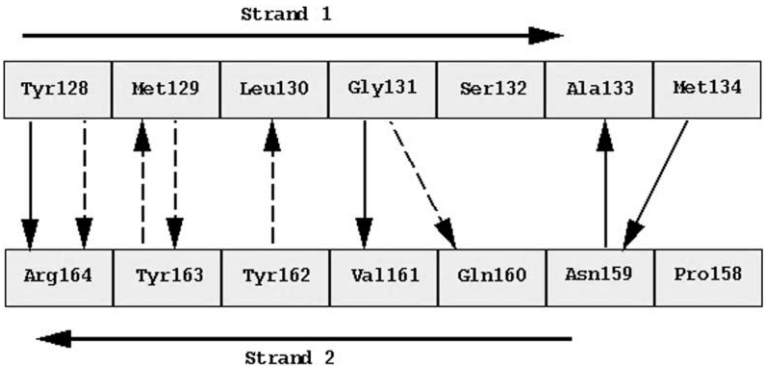

Fig. 9. A diagram representing the original hydrogen bonds (dotted arrows) and the new hydrogen bonds (solid arrows) formed in the β-sheet during the Asp178Asn mutant simulation at 500 K.

The initial and new hydrogen bonds in the sheet are shown schematically in Fig. 9.

It has been suggested that the β-sheet region of the PrP^C may be the nucleation site for the conformational transition to the infectious form of the prion protein, PrP-res for which an increased β-sheet content is expected [35]. From the above results, it may be possible that the Asp178Asn mutation allows formation of a more extended β-sheet structure which might facilitate or accelerate the conversion to the diseased form.

At 500 K, in addition to elongation of the β-sheet, disruption of the protein tertiary structure occurred. After 800 ps, the loop connecting strand 1 to helix 1 moved, leaving a gap in the tertiary structure of the protein (this was supported by the high RMSD and high radius of gyration changes after 800 ps of the simulation). This change in the loop conformation could be a point on the pathway of prion protein misfolding. Extending the simulation time or using a different technique for calculating non bonded electrostatic interactions (see later for a possible problem with PME) could reveal more changes and may be able to give insight about the pathway for conversion of normal to abnormal prion protein.

4. Discussion

The PME method appeared to be the best method to give a stable simulation for the prion protein at 300 K. Using the NMR structure of the prion protein as starting point gave more stable simulations for wild-type protein. The wild type homology models tended to become closer structurally to the human NMR structure, validating the methodology to some extent. It should be noted that the prion protein is glycosylated. One of the points of glycosylation is Asn181 which is near to the point of mutation. Glycosylation is likely to affect the local conformation of the protein [25].

The secondary structure of the wild type protein remains reasonably stable at both 300 and 500 K. The only significant difference being a temporary gain in β-sheets content.

However, the Asp178Asn mutant shows a more significant increase in β-sheet content, which was more pronounced at 500 K. This may be part of the pathway followed during the conversion of normal prion protein to the abnormal protein. In addition, at 500 K, further breakdown of the structure occurred.

Interestingly, the simulation of the human NMR structure appeared stable even at 500 K. This contrasts to simulations reported on other proteins which generally lead to some unfolding. There could be two reasons for this. Firstly, the prion protein may have high thermal stability due to a large number of salt bridges on the surface: it is reported that prion protein possess three salt bridges (Glu146–Arg208, Arg164–Asp178, and Arg156–Glu196) and a disulfide bond that connects helix 2 and helix 3 which contribute to prion protein stability [23]. Two of these salt bridges involve disease-associated mutations. Tracing the distance between the carboxylate oxygen of Asp178 and the guanidine nitrogen of Arg164, and between those of Arg208 and Glu146 in both of the 300 and 500 K simulations based on the NMR structure, showed conservation of these salt bridges during the simulation. In the NMR structure, Arg208 and Glu146 were far away from each other, but during the 300 K simulation they moved close enough for electrostatic interactions. This was achieved more rapidly in the high temperature simulation, as the high temperature enables the protein to overcome energy barriers. The Arg156–Glu196 salt bridge and the disulfide bond were conserved during the PME simulation of the human NMR structure. Several experiments confirm that salt bridges do stabilise the proteins at elevated temperatures. For example, the importance of a salt bridge (Glu34–Lys38) for the stability of the thermostable DNA-binding protein HU from *Bacillus streyhikk* was proved experimentally by site-directed mutagenesis [36]. Liemann and Glockshuber [37] have studied the influence of amino acid substitution on the thermodynamic stability of the cellular prion protein. Their work indicates that not all the variants have lowered the thermodynamics stability than the wild type, but the Asp178Asn mutation lowers the thermodynamics stability by about 7.2 ± 1.7 kJ/mol from the wild type, and the Arg208His mutation lowers it about 6.0 ± 2.5 kJ/mol. This drop in thermodynamics stability upon these two mutations, presumably due to loss of salt bridge formation, leads to protein thermal instability. These results can support our hypothesis that the salt bridges in the prion protein may play an important rule in its high thermal stability.

Secondly, the stability of the simulation may be due to an artefact of the Particle Mesh Ewald method. Reported dynamics studies on unfolding of proteins have used the cut-off method of electrostatic calculation interaction [38–40]. However, the PME method may super stabilise the protein at elevated temperature and so delays its unfolding [41]. De Bakker et al. [42] have found similar thermal stability for the protein Sac7d upon using PME method for calculating long range electrostatic interactions in their molecular dynamics simulation.

5. Conclusion

The Particle Mesh Ewald method has provided a way to undertake molecular dynamics simulations of the prion protein. This has revealed high structural stability of the wild type protein, although some of this stability may be due to an artefact of the PME method of calculating non-bonded electrostatic interactions. The study with a Asp178Asn mutant revealed an increase in β-sheet content, due to movement of the loop regions. This may be related to the mechanism of transformation of normal to abnormal prion protein. Chemical entities which can stabilise the prion protein by preventing movement of the loop or by fitting the area between the two strands forming the β-sheet and so prevents its elongation may have therapeutic utility in the prevention of prion diseases.

Acknowledgements

We should like to acknowledge the government of Egypt and the Cardiff Centre for Molecular Modelling for support and Mr Les Craven for technical support.

References

[1] M.E. Bruce, R.G. Will, J.W. Ironside, I. McConnell, D. Drummond, A. Suttie, L. McCardle, A. Chree, J. Hope, C. Birkett, S. Cousens, H. Fraser, C.J. Bostock, Transmissions to mice indicate that new variant CJD is caused by the BSE agent, Nature 389 (1997) 498–501.
[2] A.F. Hill, M. Desbruslais, S. Joiner, The same prion strain causes vCJD and BSE, Nature 389 (1997) 448–450.
[3] N. Stahl, D.R. Borchelt, S.B. Prusiner, Differential release of cellular and scrapie prion proteins from cellular membranes by phosphatidylinositol-specific phospholipase-C, Biochemistry 29 (1990) 5405–5412.
[4] N. Stahl, M.A. Baldwin, D.B. Teplow, L. Hood, B.W. Gibson, A.L. Burlingame, S.B. Prusiner, Structural studies of the scrapie prion protein using mass spectrometry and amino-acid sequencing, Biochemistry 32 (1993) 1991–2002.
[5] R. Riek, S. Hornemann, G. Wider, M. Billeter, R. Glockshuber, K. Wuthrich, NMR structure of the mouse prion protein domain PrP(121–231), Nature 382 (1996) 180–182.
[6] R. Riek, S. Hornemann, G. Wider, R. Glockshuber, K. Wuthrich, NMR characterization of the full-length recombinant murine prion protein, mPrP(23–231), FEBS Lett. 413 (1997) 282–288.
[7] T.L. James, H. Liu, N.B. Ulyanov, S. FarrJones, H. Zhang, D.G. Donne, K. Kaneko, D. Groth, I. Mehlhorn, S.B. Prusiner, F.E. Cohen, Solution structure of a 142-residue recombinant prion protein corresponding to the infectious fragment of the scrapie isoform, Proc. Natl. Acad. Sci. U.S.A. 94 (1997) 10086–10091.
[8] R. Zahn, A.Z. Liu, T. Luhrs, R. Riek, C. von Schroetter, F.L. Garcia, M. Billeter, L. Calzolai, G. Wider, K. Wuthrich, NMR solution structure of the human prion protein, Proc. Natl. Acad. Sci. U.S.A. 97 (2000) 145–150.
[9] F.L. Garcia, R. Zahn, K. Wuthrick, NMR Structure of the bovine prion protein, Proc. Natl. Acad. Sci. U.S.A. 97 (2000) 8334–8339.
[10] L. Calzolai, D.A. Lysek, P. Guntert, C.V. Schroetter, R. Riek, R. Zahn, NMR Structure of three single-residue variants of the human prion protein, Proc. Natl. Acad. Sci. U.S.A. 97 (2000) 8341–8345.

[11] J. Stockel, J. Safar, A.C. Wallace, F.E. Cohen, S.B. Prusiner, Prion protein selectively binds copper(II) ions, Biochemistry 37 (1998) 7185–7193.
[12] R. Koradi, M. Billeter, K. Wuthrich, MOLMOL: a program for display and analysis of macromolecular structures, J. Mol. Graph. 14 (1996) 51.
[13] N.N. Stahl, S.B. Prusiner, Prions and prion proteins, Faseb J. 5 (1991) 2799–2807.
[14] K.M. Pan, M. Baldwin, J. Nguyen, M. Gasset, A. Serban, D. Groth, I. Mehlhorn, Z.W. Huang, R.J. Fletterick, F.E. Cohen, S.B. Prusiner, Conversion of α-helices into β-sheets features in the formation of the scrapie prion proteins, Proc. Natl. Acad. Sci. U.S.A. 90 (1993) 10962–10966.
[15] R.K. Meyer, M.P. McKinley, K.A. Bowman, M.B. Braunfeld, R.A. Barry, S.B. Prusiner, Separation and properties of cellular and scrapie prion proteins, Proc. Natl. Acad. Sci. U.S.A. 83 (1986) 2310–2314.
[16] D.R. Borchelt, M. Scott, A. Taraboulos, N. Stahl, S.B. Prusiner, Scrapie and cellular prion proteins differ in their kinetics of synthesis and topology in cultured-cells, J. Cell Biol. 110 (1990) 743–752.
[17] S.B. Prusiner, Chemistry and biology of prions, Biochemistry 31 (1992) 12277–12288.
[18] F.E. Cohen, K.M. Pan, Z. Huang, M. Baldwin, R.J. Fletterick, S.B. Prusiner, Structural clues to prion replication, Science 264 (1994) 530–531.
[19] K. Kaneko, L. Zulianello, M. Scott, C.M. Cooper, A.C. Wallace, T.L. James, F.E. Cohen, S.B. Prusiner, Evidence for protein X binding to a discontinuous epitope on the cellular prion protein during scrapie prion propagation, Proc. Natl. Acad. Sci. U.S.A. 94 (1997) 10069–10074.
[20] J.S. Griffith, Self replication and scrapie, Nature 215 (1967) 1043–1044.
[21] V. Daggett, M. Levitt, Realistic simulations of native-protein dynamics in solution and beyond, Annu. Rev. Biophys. Biomolec. Struct. 22 (1993) 353–380.
[22] L. Aijun, V. Daggett, Identification and characterisation of the unfolding trasition state of chymotrypsin inhibitor 2 by molecular dynamics simulation, J. Mol. Biol. 257 (1996) 412–429.
[23] J. Zuegg, J.E. Greedy, Molecular dynamics simulations of human prion protein: importance of correct treatment of electrostatic interactions, Biochemistry 38 (1999) 13862–13876.
[24] C. Guilbert, F. Ricard, J.C. Smith, Dynamic simulation of the mouse prion protein, Biopolymers 54 (2000) 406–415.
[25] N.K.C. Wong, D.V. Renouf, S. Lehmann, E.F. Hounsell, Glycosylation of prions and its effect on protein conformation relevant to amino acid mutations, J. Mol. Graphics Mod. 18 (2000) 126–134.
[26] O. Parchment, J. Essex, Molecular dynamics of mouse and Syrian hamster PrP: implication for activity, Proteins 38 (2000) 327–340.
[27] Sybyl 6.5, Tripos Inc., 1699 South Hanley Road, St Louis, Missouri 63144, USA.
[28] D. Pearlman, D. Case, J. Caldwell, W. Ross, T. Cheatham, S. DeBolt, D. Ferguson, G. Seibel, P. Kollman, AMBER, a computer program for applying molecular mechanics normal mode analysis: molecular dynamics and free energy calculations to elucidate the structures and energies of molecules, Comput. Phys. Commun. 91 (1995) 1–41.
[29] D. Case, D. Pearlman, J. Caldwell, T. Cheatham, W. Ross, C. Simmerling, T. Darden, K. Merz, R. Stanton, A. Cheng, J. Vincent, M. Crowley, D. Ferguson, R. Radmer, G. Seibel, U. Singh, P. Weiner, P. Kollman, AMBER5, University of California, San Francisco, 1997.
[30] W. Cornell, P. Cieplak, G. Bayly, I. Gould, K. Merz, D. Ferguson, D. Spellmeyer, T. Fox, J. Caldwell, P. Kollman, A second generation force field for the simulation of proteins, nucleic acids and organic molecules, J. Am. Chem. Soc. 117 (1995) 5179–5197.
[31] W. Jorgensen, J. Chandreskhar, J. Madura, R. Imprey, M. Klein, Comparison of simple potential functions for simulating water, J. Chem. Phys. 79 (1983) 926–935.
[32] H.J.C. Berendsen, J.P.M. Postma, W.F. Vangunsteren, A. Dinola, J.R. Haak, Molecular-dynamics with coupling to an external bath, J. Chem. Phys. 81 (1984) 3684–3690.
[33] J.P. Ryckaert, G. Ciccohi, H. Berendsen, Numerical integration of the cartesian equations of motion of a system with constraints, Mol. Dyn. Alkanes 23 (1997) 327–341.
[34] D.M. York, T.A. Darden, L.G. Pedersen, M.W. Anderson, Molecular-dynamics simulation of HIV-1 protease in a crystalline environment and in solution, Biochemistry 32 (1993) 1443–1453.
[35] R. Glockshuber, S. Hornemann, R. Riek, G. Wider, M. Billeter, K. Wuthrick, The three-dimensional NMR structure of a self-folding domain of the prion protein PrP(121–231), Trends Biochem. Sci. 22 (1997) 241–242.
[36] S. Kawamura, I. Tanaka, H. Kimura, Contribution of a salt bridge to the thermostability of DNA binding protein HU from *Bacillus stearothermophilus* determined by site-directed mutagenesis, Biochemistry 121 (1997) 448–455.
[37] S. Liemann, R. Glockshuber, Influence of amino acid substitutions related to inherited human prion diseases on thermodynamic stability of the cellular prion protein, Biochemistry 38 (1999) 3258–3267.
[38] A. Caflisch, M. Karplus, Acid and thermal denaturation of barnase investigated by molecular dynamics simulations, J. Mol. Biol. 252 (1995) 672–708.
[39] A.J. Li, V. Daggett, Molecular dynamics simulation of the unfolding of barnase: characterisation of the major intermediate, J. Mol. Biol. 275 (1998) 677–694.
[40] P. Ferrara, J. Apostolakis, A. Caffisch, Computer simulation of protein folding by targeted molecular dynamics, Proteins 39 (2000) 252–260.
[41] P. Hunenberger, J.A. McCammon, Effect of artificial periodicity in simulations of biomolecules under Ewald boundary conditions: a continuum electrostatics study, Biophys. Chem. 78 (1999) 69–88.
[42] P. De Bakker, P. Hunenberger, J. McCammon, Molecular dynamics simulations of the hyperthermophilic protein Sac7d from *Sulfolobus acidocaldarius*: contributions of salt bridges to thermostability, J. Mol. Biol. 285 (1999) 1811–1830.